NANO LETTERS

Letter

pubs.acs.org/NanoLett

Sb-Induced Phase Control of InAsSb Nanowires Grown by Molecular Beam Epitaxy

Q. D. Zhuang,*[,†,‡] Ezekiel A. Anyebe,[‡] R. Chen,[§] H. Liu,[∥] Ana M. Sanchez,[⊥] Mohana K. Rajpalke,[#] Tim D. Veal,[#] Z. M. Wang,*[,‡] Y. Z. Huang,[∥] and H. D. Sun[▽]

[†]Institute of Fundamental and Frontier Sciences, University of Electronic Science and Technology of China, Chengdu 610054, People's Republic of China

[‡]Physics Department, Lancaster University, Lancaster LA1 4YB, United Kingdom

[§]Department of Electrical and Electronic Engineering, South University of Science and Technology of China, Shenzhen, Guangdong 518055, People's Republic of China

[∥]School of Materials Science and Engineering, Nanyang Technological University, 50 Nanyang Avenue, Singapore 639798, Singapore

[⊥]Department of Physics, University of Warwick, Coventry CV4 7AL, United Kingdom

[#]Stephenson Institute for Renewable Energy and Department of Physics, University of Liverpool, Liverpool L69 7ZF, United Kingdom

[▽]Division of Physics and Applied Physics, School of Physical and Mathematical Sciences, Nanyang Technological University, Singapore 637371, Singapore

Supporting Information

ABSTRACT: For the first time, we report a complete control of crystal structure in $InAs_{1-x}Sb_x$ NWs by tuning the antimony (Sb) composition. This claim is substantiated by high-resolution transmission electron microscopy combined with photoluminescence spectroscopy. The pure InAs nanowires generally show a mixture of wurtzite (WZ) and zinc-blende (ZB) phases, where addition of a small amount of Sb (~2−4%) led to quasi-pure WZ InAsSb NWs, while further increase of Sb (~10%) resulted in quasi-pure ZB InAsSb NWs. This phase transition is further evidenced by photoluminescence (PL) studies, where a dominant emission associated with the coexistence of WZ and ZB phases is present in the pure InAs NWs but absent in the PL spectrum of $InAs_{0.96}Sb_{0.04}$ NWs that instead shows a band-to-band emission. We also demonstrate that the Sb addition significantly reduces the stacking fault density in the NWs. This study provides new insights on the role of Sb addition for effective control of nanowire crystal structure.

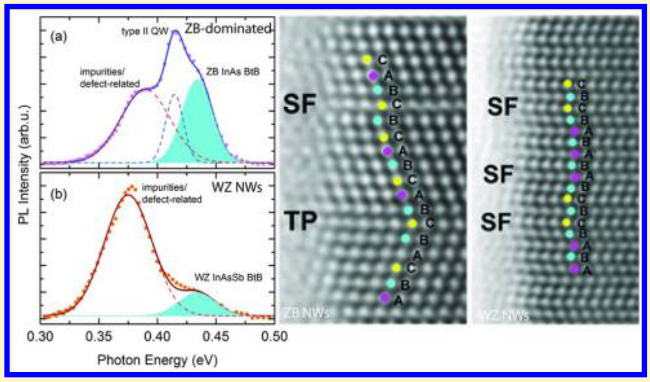

KEYWORDS: *InAsSb, nanowires, phase, molecular beam epitaxy, TEM, SEM, photoluminescence*

Semiconducting nanowires (NWs) have recently shown great promise for fabrication of novel high-performance photonic and nanoelectronic devices such as light emitting diodes,[1] detectors,[2] solar cells,[3] lasers,[4] and transistors.[5] Consequently, they have been the focus of research activities of semiconductors and nanotechnology in the past decade. However, the maximal exploitation of NWs geometry for future high-performance nanodevices is threatened by the existence of wurtzite/zinc blende (WZ/ZB) phase mixtures (polytypes) and structural defects that degrade their optical and electrical properties.[6] The coexistence of these polytypes have been shown to modify the electronic band structure leading to significant discrepancies in optical band gap values[7−10] with enormous challenges for device applications.[11] In addition, it has been demonstrated that these polytypes exhibit higher resistivity (2 orders of magnitude) than that of single-phase NWs that is detrimental to carrier transport and device functionalities.[12] As a result, the control over crystal phase purity is considered as one of the key challenges of III−V NWs for device applications.[13,14] In the past few years, much effort has been devoted to control WZ/ZB polytypism through a number of manners including tuning NWs diameter,[15,16] optimizing growth parameters such as growth temperature,[15,17,18] III/V flux ratio[17,18] and supersaturation,[19] as well as changing the type of catalyst.[13]

Most recently, it has been demonstrated that incorporation of minute concentration of impurities and dopants induces structural phase changes. For instance, selenium has been

Received: October 24, 2014
Revised: December 16, 2014
Published: January 5, 2015

DOI: 10.1021/nl5040946
Nano Lett. 2015, 15, 1109−1116

reported to promote a structural transformation in InAs NWs,[20] and zinc has triggered a WZ → ZB phase transition in InP NWs.[21,22] Antimony (Sb) as a typical surfactant Sb has also been reported to modify the structural property of III−V semiconductor materials even if at an undetectable concentration. Both minute Sb incorporation and Sb-rich growths have demonstrated a change of crystal structure from WZ to ZB in InAs NWs and InAs/InSb NWs heterostructures.[6,23] It has also been reported that the presence of very small amount of Sb in InAs nanowires leads to a change in crystal structure from pure WZ to pure ZB via intermediate stacking fault and pseudoperiodic twinning regimes in InAs/$InAs_{1-x}Sb_x$ heterostrcutures.[24] In addition, a WZ → ZB phase change has been demonstrated in both GaAs/$GaAs_xSb_{1-x}$/GaAs NWs heterostructures[25] and GaAs NWs.[26] However, most of these reports are limited to Au-catalyzed NWs. Given the huge potential of self-catalyzed (SC) NWs for future device integration with Si and the enormous benefit derivable in crystal-phase-engineered NW, an investigation of the role of impurities in phase control of SC NWs is essential.[6] Furthermore, the introduction of impurities also enables band gap engineering for NWs characteristics and device functionalities. It is of particular interest to incorporate Sb InAs NWs that results in ternary $InAs_{1-x}Sb_x$ NWs. These NW materials having widely tunable band gap covering the whole infrared spectrum and high carrier mobility, consequently hold promises in fabricating infrared emission and detection[24] as well as high-speed electronics.[27]

There is rare investigation of the influence of Sb addition to crystal phase of $InAs_{1-x}Sb_x$ NWs given the limited report of $InAs_{1-x}Sb_x$ NWs growth in literature. Only recently, Sourribes et al.[28] reported the catalyst-free growth of InAs/$InAs_{1-x}Sb_x$ NWs heterostructures ($3.9 \leq x \leq 15.4$) on Si. A phase change from WZ dominant InAs NWs to quasi-pure ZB $InAs_{0.85}Sb_{0.15}$ NWs was observed. Given the significant influence of undetectable Sb content on NWs structures, an investigation of the presence of very small Sb incorporation into InAs NWs is essential to understand the effect of Sb on the growth. Aiming to elucidate the influence of trace Sb content (~2%) on the crystal structure of InAs NWs grown directly on Si, we report the Sb-induced control of crystal phase in SC $InAs_{1-x}Sb_x$ NWs with Sb composition spanning from low level (as low as ~2%) to a value up to ~10%. We observed a remarkable evolution from a polytypic crystal to a quasi-pure WZ phase structure and quasi-pure ZB phase structure with increase of Sb incorporation, which are accompanied by a significant reduction in stacking fault (SF) density. Detailed composition dependent photoluminescence (PL) from these $InAs_{1-x}Sb_x$ NWs with different phase mixtures is also reported for the first time.

Experimental Details. $InAs_{1-x}Sb_x$ NWs growth was performed on bare Si(111) substrate by molecular beam epitaxy (MBE) via a droplet-assisted growth.[29] The Si substrate was initially activated by In droplets to create favorable nucleation sites, then the NWs were grown at preoptimized conditions with growth temperature in the range of 420−460 °C under As-rich condition with a fixed As_4 beam equivalent pressure (BEP) of around 5.8×10^{-6} mbar. The Sb BEP was varied to control the Sb incorporation. The samples were grown in growth duration of 20−120 min. The growth was terminated by closing all the shutters simultaneously. A reference InAs NWs sample was grown on bare Si(111) substrate at identical conditions without presence of Sb flux. The incorporated Sb content in the samples was estimated by using combination of X-ray diffraction and energy-dispersive X-ray spectroscopy (EDX) measurements. The X-ray measurements were performed on as-grown samples. To further verify the Sb incorporation into the NWs, FEI XL30 SFEG scanning electron microscope (SEM) was utilized to determine the Sb composition. The EDX measurements were taken from top on both single NWs and clusters. Sb composition along NW at different positions was also measured from side with the samples tilted by 45° to minimize the effect from the clusters (see Supporting Information for details). The surface morphology of the NWs was obtained by SEM. The microstructure of NWs was characterized using JEOL 2100 LaB_6 and 2100F microscopies at beam energy of 200 kV. The specimens were prepared using conventional method through the transformation of NWs onto a TEM holey carbon grid from a suspension solution with NWs. The analysis was carried out with the electron beam perpendicular to the growth direction and parallel to the $\langle 110\rangle_{ZB}/\langle 11{-}20\rangle_{WZ}$ direction. Low-temperature (10 K) photoluminescence (PL) measurement was also performed on the as-grown samples to investigate the optical properties of the InAsSb NWs. A diode laser at wavelength of 980 nm was used for excitation of the sample with a laser power density of ~20 W/cm^2, and the emission signal was detected using a liquid nitrogen cooled InSb photodiode detector with a standard digital lock-in amplifier technique.

Figure 1 depicts the SEM images of $InAs_{1-x}Sb_x$ NWs with varying Sb compositions. The Sb content (x_{sb}) in $InAs_{1-x}Sb_x$ NWs samples were estimated by EDX measurements as ~0, 2, 4, and 10% (samples A−D). It clearly shows a significant modification on the average diameter (from ~48 to 75, 109, and 155 nm) owing to the addition of Sb as described previously.[30]

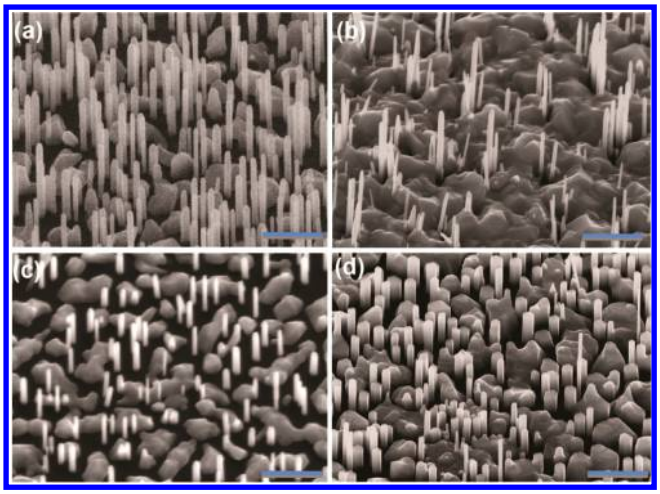

Figure 1. The 45°-tilted SEM images of vertically aligned $InAs_{1-x}Sb_x$ NWs with varying Sb molar fraction (x_{sb}) of ~0% (a); 2% (b); 4% (c); and 10% (d). The scale bar for all images is 1 μm.

Structural Characterization of $InAs_{1-x}Sb_x$ Nanowires. In order to quantify distribution of polytypes and crystal defects in the NWs, we employed high-resolution transmission electron microscopy (HRTEM) to evaluate the resulting InAsSb NWs at varying Sb compositions. III−V semiconductor NWs usually crystallizes in both WZ and ZB phases so the NWs always exhibit a mixture of phases with presence of planar defects. We simply classify the defects into three categories: stacking fault (SF), rotational twin-plane (TP), and polytype boundary (PB).

DOI: 10.1021/nl5040946
Nano Lett. 2015, 15, 1109−1116

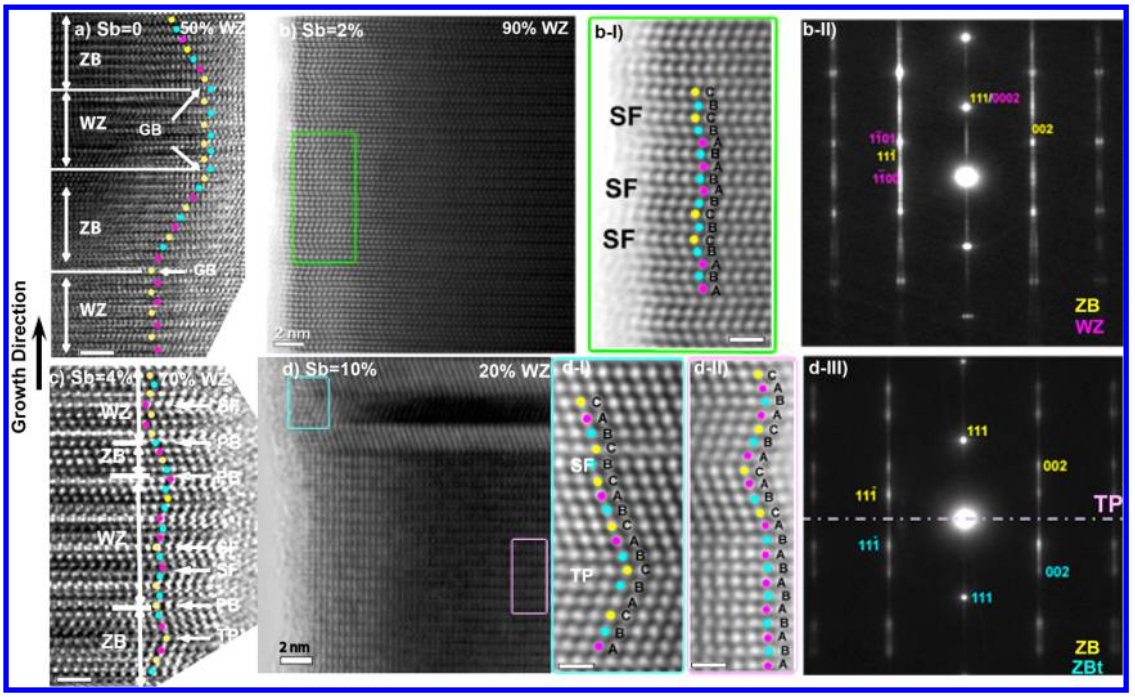

Figure 2. High-resolution TEM (HRTEM) images of $InAs_{1-x}Sb_x$NWs with Sb content of (a) 0, (b) 2, (c) 4, and (d) 10%. The InAs NWs (Sb content of 0%) have a ZB dominant structure with WZ fraction of 20%. Addition of Sb with content of 2% and 4% resulted in WZ predominant phase, while further increase of Sb content (10%) led to ZB predominant structure. Magnified HRTEM image of the highlighted region of sample (b) is shown in (b-I) with the corresponding fast Fourier transform (FFT) pattern showing in (d-II). Magnified HRTEM images of the highlighted regions of sample (d) is shown in (d-I) with the corresponding FFT pattern showing in (d-III). These magnified images show the stacking in the structure revealing ZB and WZ structures and SF and TP. The scale bar is 1 nm.

The SFs are partial displacements affecting the regular sequence in the stacking of the lattice planes caused by either a vacant plane (intrinsic SF) or an insertion of extra plane (extrinsic SF). The TPs are planes where the crystal is rotated by 60°. The PBs are the planes between ZB and WZ phases whose density implies the size of segment of the phases. We did not count this density in our defect density analysis. In order to estimate the phase percentage in the NWs, we adopt the metrics proposed by Caroff et al. in which the segment containing at least four consequences of stacking sequences can be treated as a specific crystal phase. The percentage of WZ phase in the NWs was deduced from analysis of many HRTEM images of multiwires for each sample. Figure 2 shows the HRTEM images of the samples of reference InAs NWs and InAsSb NWs with Sb composition of ∼2, 4, and 10%. It can be seen from Figure 2a that the reference InAs NWs exhibit a polytypic ZB/WZ crystal structure (∼50% WZ) along with defects of PBs and low density of SFs and TPs (present in other images). This behavior is typical in SC InAs NWs[31−33] and can be understood by means of contribution of lateral surfaces to the total free energy during growth. Bulk III−V materials with the highest ionicity such as the III-Nitrides often adopt the WZ phase whereas the ZB phase is favored in other III−V materials. However, most of other III−V NW materials including InAs, InP, GaAs, and GaP have moderate ionicity values generally lead to a strong tendency for the formation of SFs, TPs, and polytypism, which are independent to the growth synthesis methods.[6,34] As a result, InAs NWs often show sequential mixtures of ZB and WZ phases (polytypes). This is significantly pronounced in SC NWs that the ZB structure is the most predominant phase.[31−33] However, the favorable phase was reported to be sensitive to the surface-to-volume ratio.[11,16] The WZ phase has a lower surface energy in comparison to the corresponding crystalline orientation of the same ZB material owing to its smaller third-nearest-neighbor atom spacing (resulting from its distinct stacking sequence), as a consequence the WZ phase is more stable in NWs structures with high surface-to-volume ratio. The occurrence of polytypes in ZB III−V NWs is often associated with the small radius of NWs, resulting in a large relative contribution of lateral surfaces to the total free energy of fully formed NWs.[35]

The sample of InAsSb NWs with Sb composition of ∼2% (Figure 2b) shows a WZ-predominant crystal structure (90%). This dramatic crystal change from ZB-predominant in InAs to WZ-predominant structure is attributed to the trace Sb incorporation that has not been observed previously. A magnified HRTEM image of a WZ phase section is shown in Figure 2 b-I. Stacking corresponding to WZ structure (··· ABAB··· and ···CBCB···) and intrinsic SFs (ABAB CBCB) were revealed in this image. The quasi-pure WZ structure of the NWs is corroborated by the corresponding fast Fourier transform (FFT) electron diffraction pattern as depicted in Figure 2b-II. The 111_{ZB} and/or 0002_{WZ} spot indicates the growth direction both in ZB and WZ phases. It clearly shows that the WZ reflections are more intense than that of ZB ones that further confirm the dominant WZ structure. The streaks passing through the spots along the growth direction indicate the presence of stacking faults in the structure, lying on the $(111)_{ZB}/(0002)_{WZ}$ planes. The sample of InAsSb NWs with higher Sb composition of 4% (Figure 2c) still exhibits a quasi-pure WZ structure with decreasing portion (70%). This observation contradicts previous report on catalyst-free $InAs_{1-x}Sb_x$/InAs NWs[28] where phase transition from WZ to ZB at Sb incorporation of 3.9% was observed. The difference

DOI: 10.1021/nl5040946
Nano Lett. 2015, 15, 1109−1116

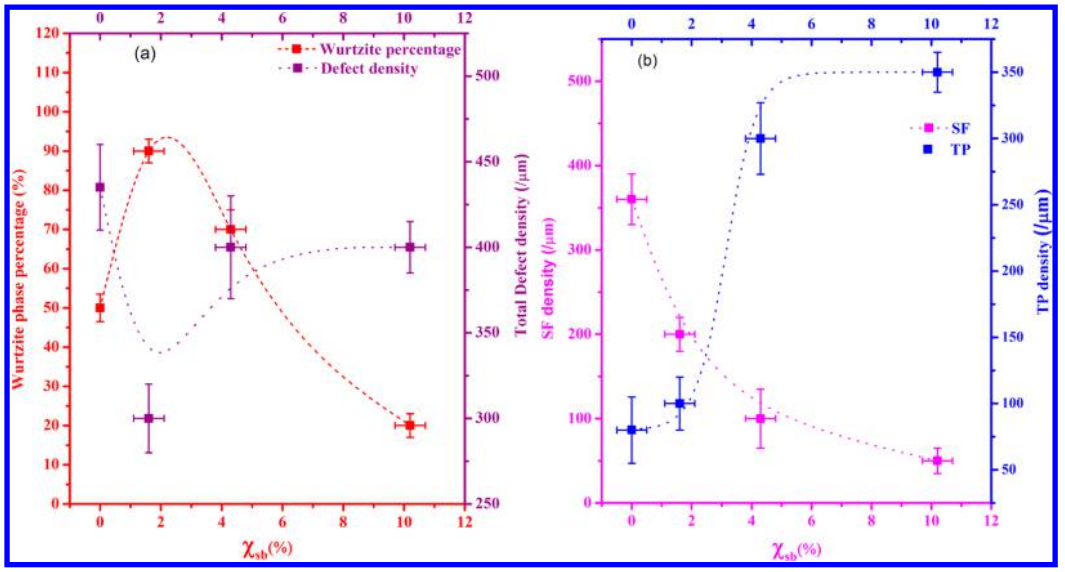

Figure 3. Plot of Wurtzite phase percentage and total defect density (a), stacking fault (SF) and twin plane (TP) density (b) in $InAs_{1-x}Sb_x$ nanowires as a function of antimony composition. The error bars stand for one standard deviation.

observed in our growth can be understood by considering differences in supersaturation[19] owing to the predeposition of indium (In) in our case against the catalyst−free growth technique. We believe that the direct deposition of our NWs on Si substrate results in differences in contact angle and diameter both of which have been recognized as crucial determinants of NWs crystal phase.[15,16] Furthermore, it is well-known that crystal phase transition can be induced by tuning growth parameters,[15,17,18] hence slight variation in growth conditions could potentially result in different crystal structure. For the sample of InAsSb NWs with further increased Sb composition of 10% (Figure 2d), surprisingly, we observed a ZB predominant structure with less WZ portion (20%). This implies a phase transition of WZ → ZB occurred at this level of Sb incorporation. Figure 2 d-I corresponds to a magnified area in the NW demonstrating mainly ZB (···ABCABC···) stacking containing twin-plan (TP) (···CBA C ABC···) and SF (··· ACBCBAC···). Areas corresponding to the WZ structure were also observed in this sample (Figure 2 d-II). This structure was corroborated by FFT pattern recorded in the NWs as shown in Figure 2 d-III. The spots in the diffraction pattern indicate that the ZB structure is predominant with presence of twinning. As before, the streaking indicates the presence of thin lamellae; it is less pronounced than that in InAsSb NWs with 2% Sb (Figure 2b-II) indicating a lower density in this sample. To further clarify the effect of Sb incorporation on the change of crystal structure in the NWs, we analyzed the TEM images for multiwires for each sample and a number of segments for each wire to determine the percentage of the crystal phases in different samples and the relevant percentage of different crystal defects, in particular, the SFs and TPs distribution in the NWs. The dependence of the percentage of the WZ crystal inclusion as a function of Sb content is plotted in Figure 3a. It clearly shows that the polytypic InAs NWs was tuned to WZ dominated InAsSb NWs with a small amount of Sb incorporation up to ∼4%, while further increase in Sb led to ZB dominated phase. In other words, the Sb incorporation offers an efficient manner in tuning the crystal phase of InAsSb NWs, via transitions of polytypic mixture → WZ → ZB along with increase of Sb incorporation.

The crystal defect density as a function of Sb composition is shown in Figure 3a. It can be seen that the crystal structure evolves from highly defective crystals in the reference InAs NWs (Sb = 0%) to less defective structures with increase of Sb addition. This is consistent with the change of FFT patterns observed in TEM study. In particular, the InAsSb NWs with 2% Sb gives minimal defect density. Intriguingly, a detailed analysis on defects reveals that the improvement of crystal quality is attributed to a significant suppression of the formation of SFs in the NWs. Figure 3b shows that the SFs density monotonically decreases with increase of Sb concentration from 360/μm in the reference InAs sample to 200/μm ($InAs_{0.98}Sb_{0.02}$), 100/μm ($InAs_{0.96}Sb_{0.04}$), and finally 50/μm ($InAs_{0.90}Sb_{0.10}$), which is consistent with previous report.[28] In stark contrast, the TPs density increased with increasing Sb incorporation as revealed in Figure 3b.

It is the first demonstration of quasi-pure WZ phase $InAs_{1-x}Sb_x$ NWs via the SC route to the best of our knowledge. Previous studies reported either a dominant ZB phase or a transition from WZ toward ZB with Sb incorporation.[28,36] This preferential crystallization of ZB phase in our $InAs_{1-x}Sb_x$ NWs[24,37−39] is believed to be associated with the fact that antimonide alloys hold the lowest ionicity among the III−V compounds. It is well established that the crystal structure of NWs is diameter dependent. The critical diameter for III−V compounds was proposed to be ∼10 nm based on thermodynamic models.[34,40] However, our NWs have much larger diameter of ∼60 to 155 nm that excludes the possibility of diameter-induced phase switching to WZ phase. We believe the surprising predominance of the WZ phase in our $InAs_{1-x}Sb_x$ NWs is associated with the In-rich growth conditions employed for our growths, which is consistent with experimental observations in SC NWs.[31,41−43] Compared to previous catalyst-free growths,[28,36] the most obvious difference in our growths is the deliberate introduction of In droplets for the preferential nucleation of NWs that favors the formation of WZ structures. Krogstrup et al.[44] have shown that the effective V/III flux ratio is the primary parameter to control the structure of NWs. This suggested that the probability of nucleating at triple phase line (TPL) may be thermodynami-

DOI: 10.1021/nl5040946
Nano Lett. 2015, 15, 1109−1116

cally favorable for In-rich conditions (described as a low As atomic fraction in the In droplet), which is in agreement with recent experimental observations.[31] The nucleation model proposed by Joyce et al.[17] revealed that changes in surface energy of the NW side facets, most importantly at the vapor−solid energy (i.e., vapor-nucleus energy), is largely responsible for ZB and WZ phase purity. They showed that the vapor−solid surface energy of the ZB nuclei is lowest at high V/III ratio (As-rich) conditions, which promote the formation of perfect TPs-free NWs. On the other hand, at low V/III ratios (In rich) conditions the WZ nuclei are likely to have lower vapor−solid surface energy than their ZB counterparts. As a result, they obtained twin-free ZB NWs at high V/III ratio due to the formation of low energy surface reconstructions that favors the nucleation and growth of ZB nanowires. On the contrary, SFs-free WZ NWs were obtained at low V/III ratio condition in which ZB surfaces are less stable. The influence of side wall facets to the prevalence of WZ phase is strongly supported by theoretical predictions.[34,45] It is therefore reasonable to assume that the appearance of WZ structures with high density of TPs is promoted by the In rich conditions at the growth front. We believe that the presence of Sb further enhances the nucleation of the WZ phase at the TPL because the increase in WZ segments correlates with the rise in x_{sb}. This suggests an increase of two-dimensional (2D) WZ nucleus nucleation probability with increase of Sb concentration in the droplet-catalyzed growth. Hence, it favors a structural transition to WZ phase that is consistent with a previous report.[40]

In order to understand the dependence of WZ phase fraction on the Sb incorporation observed in our NWs, we use the modified nucleation model proposed by Wallentin et al.[22] It is well established that $InAs_{1-x}Sb_x$ NWs exhibit diameter expansion with increasing Sb incorporation.[36,38] We recently demonstrated the surfactant effect of Sb addition to the morphology and growth of self-catalyzed InAs NWs.[30] It was shown that a trace amount of Sb flux significantly increases the NWs lateral growth and meanwhile suppresses axial growth leading to an increase in NWs diameter with a rise in Sb composition (see Figure 1). The observed changes in NWs diameter suggest an increase in droplet diameter because the diameter of NWs is well-defined by the size of predeposited indium droplets,[46,47] which would imply changes to contact angle.[22] Using Young's equation, the droplet contact angle (β) can be related to the surface energies at the TPL (Figure 4) by

$$\cos\beta = \frac{\gamma_{SV} - \gamma_{LS}}{\gamma_{LV}} \tag{1}$$

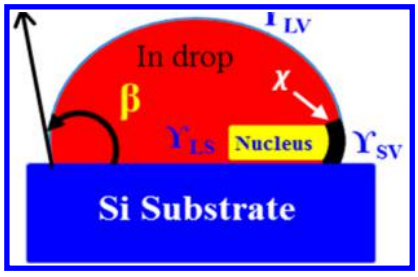

Figure 4. Schematic illustration of geometry of indium droplet on Si substrate with γ_{SV}, γ_{LS}, and γ_{LV} representing the surface energies at the solid−vapor, liquid−solid, and liquid−vapor interface, respectively, β is the contact angle between droplet and substrate, and χ is the fraction of the nucleus perimeter that is in contact with the vapor phase.

where, γ_{SV}, γ_{LS}, and γ_{LV} represent the surfaces energies at the solid−vapor, liquid−solid, and liquid−vapor interface, respectively. It is wise to conclude that an increase in Sb composition corresponds to increase in NWs diameter, which in turn results in a decrease in contact angle with respect to the substrate.[30,48] Because γ_{SV} is phase independent, we can exclude it hence focus on the critical interfacial energies only that determine the dominant crystal phase in NWs.[49,50] From eq 1, we can conclude $\cos\beta \propto (-\gamma_{LS}/\gamma_{LV})$; this indicates that an increase in NWs diameter with a corresponding decrease in contact angle would result in a decrease in the ratio of γ_{LS}/γ_{LV}. The ratio (η) between the effective surface energies of the WZ (Γ^{WZ}) and ZB (Γ^{ZB}) phase is given by[22,51]

$$\eta = \frac{\Gamma^{WZ}}{\Gamma^{ZB}} = \frac{(1-x)\gamma_{LS}^{1} - x\gamma_{LV}\sin\beta + \tau x\gamma_{wz}}{(1-x)\gamma_{LS}^{1} - x\gamma_{LV}\sin\beta + x\gamma_{ZB}} \tag{2}$$

where x is the fraction of the nucleus perimeter that is in contact with the vapor phase, and $\tau = \gamma_{WZ}/\gamma_{ZB}$ is the ratio of the lateral solid−vapor surface energies of WZ and ZB NWs in contact with the vapor. A necessary condition for the formation of NWs in WZ phase is $\tau < 1$ because of the presence of less dangling bonds on the WZ surface.[14,22,51] The ratio (ξ) between the WZ (ΔG_{WZ}) and ZB (ΔG_{ZB}) nucleation barriers is expressed as[22,50]

$$\xi = \frac{\Delta G_{WZ}}{\Delta G_{ZB}} = \frac{\Delta\mu_{LS}\eta^2}{\Delta\mu_{LS} - \Psi_{WZ}} \tag{3}$$

where $\Delta\mu_{LS}$ is supersaturation at the liquid−solid interface and Ψ_{WZ} is additional cohesive energy required for the formation of a WZ layer at the TPL, thus representing the comparatively low cohesive energy of ZB phase. As can be seen from eq 3, the layer by layer deposited NWs would adopt the WZ structure when $\xi < 1$, which would imply $\eta \ll 1$. As a consequence, a significant lowering of γ_{LS} or increase in γ_{LV} will promote a decrease in both η and ξ, favor the WZ phase nucleation probability. Thus, the WZ phase is preferentially formed at the TPL when its nucleation barrier is lower than that of its ZB counterpart, although the latter is more stable in bulk form.[13,14] In addition, the incorporation of increased Sb composition in NWs possibly results in modification to the surface energetics at the γ_{LS} and/or γ_{LV} interface, as a consequence leads to a ZB → WZ phase transition as reported previously.[40,52] Surfactants have been recognized as crucial elements for engineering NWs crystal and defect structure.[49] However, the decline in the WZ fractions at high Sb content (x_{sb} = 10%) is likely associated with modifications to the balance of forces and/or changes to the V/III flux ratio that is a complication of Sb surfactant effect.[36,53] This suggests that the Sb-induced tuning of crystal phase is composition dependent. Because the required condition for WZ phase formation involves altering the balance of surface energies, an appropriate choice and composition of surfactants would enable the control of the preferred crystal phases in NWs.

Optical Properties of the $InAs_{1-x}Sb_x$ NWs Nanowires. Because there is significant structural evolution of InAsSb NWs with increase of Sb incorporation, it is extremely interesting to elucidate the optical properties of these InAsSb NW ensembles. We performed low-temperature (10 K) photoluminescence (PL) measurement on the as-grown samples. The typical PL spectrum of the reference InAs NWs and the $InAs_{0.96}Sb_{0.04}$ NWs are depicted in Figure 5a,b, respectively. It can be seen

DOI: 10.1021/nl5040946
Nano Lett. 2015, 15, 1109−1116

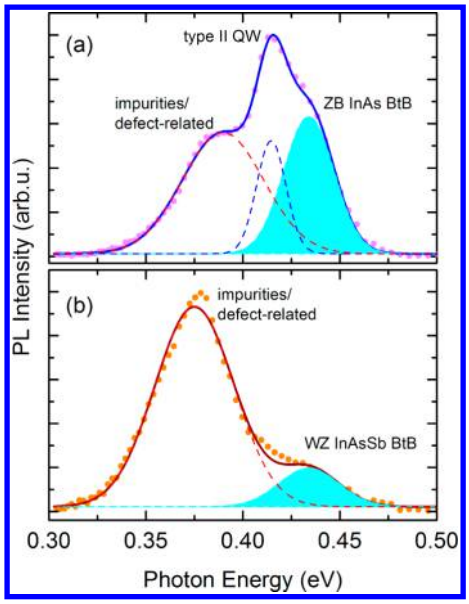

Figure 5. PL spectra of (a) InAs and (b) $InAs_{0.96}Sb_{0.04}$ NWs at 10 K. The sample of InAs NWs shows three emission peaks with an emission that is related to the transition of type II QWs formed from the mixture of WZ and ZB phases, while the sample of $InAs_{0.96}Sb_{0.04}$ NWs clearly exhibits a BtB associated emission from WZ phase without the presence of type II QW emission, which indicates the quasi-pure WZ phase in the InAsSb NWs.

that the InAs NWs show a multipeak emission. The decomposition indicates three emissions centered at ∼0.389, 0.415, and 0.434 eV. The lowest emission is attributed to the impurity or defect-related transition,[54−57] while the dominant emission centered at 0.415 eV is associated with the presence of the WZ/ZB mixture, and the emission at the largest energy is due to the band-to-band (BtB) transition from ZB InAs. The mixture of WZ and ZB InAs sections forms a type II related quantum wells (QW), where electrons confined in the QWs of the ZB segments and holes localized in the WZ regions.[58,59] Optically excited electrons undergo a transition from the ground state in the ZB conduction band to the top of the WZ valence band followed by radiative recombination[7] (type II QW related emission). The corresponding radiative recombination to the observed optical emission is schematically illustrated in Figure 6. The energy of the emission from this type II QW transition (0.415 eV) is in good agreement with previous report on polytypic InAs NWs.[7]

For the sample of $InAs_{0.96}Sb_{0.04}$ NWs, the PL spectrum only shows two emission peaks; one is at 0.375 eV and the other is at 0.437 eV, which are attributed to impurity or defects-related transition and BtB transition in WZ InAsSb, respectively.

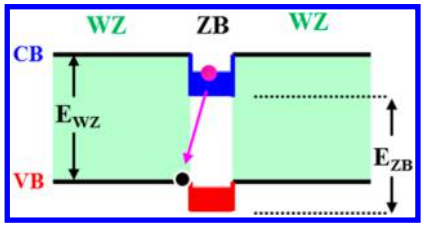

Figure 6. Schematic diagram of band alignment and recombination processes for carriers transiting between valence band and conduction band in InAs NW containing mixture of WZ and ZB phases.

Intriguingly, the emission associated with type II QW transition observed in InAs NWs is absent in this sample. This observation is in good agreement with the HRTEM studies where the NWs crystal structure evolves from the highly polytypic crystal to a quasi-pure WZ crystal with Sb incorporation. This is a further evidence of the phase transition to quasi-pure WZ phase in $InAs_{0.96}Sb_{0.04}$ NWs. It is sensible that the type II QW transition in InAs NWs is dominant in the PL spectrum owing to the efficient transition in QW structures. Although there are InAs(Sb) clusters deposited on Si surface, the PL emission detected on as-grown samples is believed to originate from NWs samples. This is verified by nonobservation of PL emission on the samples with the NWs removed. The nonemission of the clusters is associated with the poor material quality of these clusters resulting from the large lattice mismatch and antiphase domains. We also performed power-dependent and temperature-dependent PL measurements on the samples to further verify the origins of the emission peaks (the results are given in the Supporting Information). From these detailed PL measurements, the assignments of the peaks are fully confirmed. It is worth noting that the BtB emission from InAs NWs at ∼0.427 eV is slightly larger than the bandgap of ZB InAs (0.415 eV).[60] This larger energy could be associated with the band filling effect and size quantization in NWs. Sun et al.[54] have reported a blueshift of InAs band gap that was attributed to size-dependent quantization effects for NWs with small diameters (10−20 nm). Although our InAs NWs have a large average diameter (∼80 nm), there are also some NWs with narrower diameter that result in obvious size quantization; this is reflected by the broad PL emission.

Surprisingly, the BtB emission from the WZ $InAs_{0.96}Sb_{0.04}$ NWs centered at energy of 0.437 eV is close to that of BtB in ZB InAs NWs. This contradicts the prediction of lower bandgap energy due to the Sb incorporation. This can be interpreted by the difference of bandgap energy of different phases, for example, ZB and WZ phases. A previous report indicates that the WZ phase InAs NWs has larger bandgap energy in comparison with that of ZB InAs,[7,61,62] at a predicted value of 40−66 meV.[59,61,63] This was confirmed with an experimentally observed value of ∼0.46 eV.[7] If we assume the bandgap energy difference between WZ and ZB phases is the same for InAsSb alloys at low Sb composition, the bandgap energy of WZ InAsSb NWs can be estimated from that of ZB InAsSb. At 4.3% of Sb, ZB InAsSb alloy gives bandgap energy of 0.375 eV if a bowing effect of 0.67 eV is taken (shrinkage of 0.035 eV).[64] This gives an estimate of the bandgap energy of WZ InAsSb NWs with Sb content of 4.3% to be around 0.415−0.441 eV, which is in agreement with the energy value deduced from the PL emission. Consequently, we can confirm that the emission at 0.437 eV is due to the BtB transition from WZ InAsSb. Because of the large diameter of these NWs (∼109 nm), we expect weaker size quantization in these NWs in comparison with that of InAs NWs. It is obvious that the impurities and defects-related emission are quite strong in both samples. This could be associated with the presence of highly dense crystal twinning defects that corroborate to the earlier HRTEM and FFT results.

In summary, we have demonstrated the Sb-induced control of crystal phase mixtures in SC InAsSb nanowires. It is shown that the addition of a very small amount of Sb into InAs NWs leads to a perfectly tunable change of the crystal structure from a mixed WZ/ZB to a quasi-pure WZ phase NWs while further increase of Sb led to BZ dominated phase. We also observed

DOI: 10.1021/nl5040946
Nano Lett. 2015, 15, 1109−1116

dramatic variation in SF density as a function of Sb composition. Furthermore, optical properties of the InAsSb NWs with different phase mixtures are presented. We observed the type II QWs related emission in InAs NWs due to the coexistence of ZB and WZ phases. This emission is conspicuously absent in the $InAs_{0.96}Sb_{0.04}$ NWs, which show a clear band edge emission instead, owing to its quasi-pure WZ structure. This study provides new insights on the role of Sb addition in the control of NWs crystal phase, defects, and optical properties.

■ ASSOCIATED CONTENT

Supporting Information

Additional information including experimental details and figures. This material is available free of charge via the Internet at http://pubs.acs.org.

■ AUTHOR INFORMATION

Corresponding Authors

*E-mail: (Q.D.Z.) q.zhuang@lancaster.ac.uk.
*E-mail: (Z.M.W.) zhmwang@gmail.com.

Notes

The authors declare no competing financial interest.

■ ACKNOWLEDGMENTS

The authors would like to thank the EPSRC Lancaster Impact Acceleration Account, the Royal Society International Joint Grant, and Gas Sensing Solutions Ltd for their financial support.

■ REFERENCES

(1) Nguyen, H. P. T.; Zhang, S.; Cui, K.; Han, X.; Fathololoumi, S.; Couillard, M.; Botton, G. A.; Mi, Z. p-Type Modulation Doped InGaN/GaN Dot-in-a-Wire White-Light-Emitting Diodes Monolithically Grown on Si(111). *Nano Lett.* **2011**, *11*, 1919−1924.

(2) Svensson, J.; Anttu, N.; Vainorius, N.; Borg, B. M.; Wernersson, L. E. Diameter-Dependent Photocurrent in InAsSb Nanowire Infrared Photodetectors. *Nano Lett.* **2013**, *13*, 1380−1385.

(3) Krogstrup, P.; Jorgensen, H. I.; Heiss, M.; Demichel, O.; Holm, J. V.; Aagesen, M.; Nygard, J.; Morral, A. F. I. Single-nanowire solar cells beyond the Shockley-Queisser limit. *Nat. Photonics* **2013**, *7*, 306−310.

(4) Wang, X.; Tong, J.; Chen, X.; Zhao, B.; Ren, Z.; Li, D.; Zhuo, X.; Zhang, J.; Yi, H.; Liu, C.; Fang, F.; Li, S. Highly Ordered GaN-Based Nanowire Arrays Grown on Patterned (100) Silicon and Their Optical Properties. *Chem. Commun.* **2014**, *50*, 682−684.

(5) Colinge, J. P.; Lee, C.-W.; Afzalian, A.; Akhavan, N. D.; Yan, R.; Ferain, I.; Razavi, P.; O'Neill, B.; Blake, A.; White, M.; Kelleher, A. M.; McCarthy, B.; Murphy, R. Nanowire transistors without junctions. *Nat. Nanotechnol.* **2010**, *5*, 225−229.

(6) Caroff, P.; Bolinsson, J.; Johansson, J. Crystal phases in III-V nanowires: from random toward engineered polytypism. *IEEE J. Sel. Top. Quantum Electron.* **2011**, *17*, 829−846.

(7) Moeller, M.; de Lima, M. M., Jr.; Cantarero, A.; Chiaramonte, T.; Cotta, M. A.; Iikawa, F. Optical emission of InAs nanowires. *Nanotechnol.* **2012**, *23*, 375704.

(8) Ketterer, B.; Heiss, M.; Uccelli, E.; Arbiol, J.; Morral, A. F. I. Untangling the Electronic Band Structure of Wurtzite GaAs Nanowires by Resonant Raman Spectroscopy. *ACS Nano* **2011**, *5*, 7585−7592.

(9) Mattila, M.; Hakkarainen, T.; Mulot, M.; Lipsanen, H. Crystal-structure-dependent photoluminescence from InP nanowires. *Nanotechnology* **2006**, *17*, 1580−1583.

(10) Pemasiri, K.; Montazeri, M.; Gass, R.; Smith, L. M.; Jackson, H. E.; Yarrison-Rice, J.; Paiman, S.; Gao, Q.; Tan, H. H.; Jagadish, C.; Zhang, X.; Zou, J. Carrier dynamics and quantum confinement in type II ZB-WZ InP nanowire homostructures. *Nano Lett.* **2009**, *9*, 648−654.

(11) Dick, K. A.; Caroff, P.; Bolinsson, J.; Messing, M. E.; Johansson1, J.; Deppert, K.; Wallenberg, L. R.; Samuelson, L. Control of III−V nanowire crystal structure by growth parameter tuning. *Semicond. Sci. Technol.* **2010**, *25*, 024009.

(12) Thelander, C.; Caroff, P.; Plissard, S.; Dey, A. W.; Dick, K. A. Effects of Crystal Phase Mixing on the Electrical Properties of InAs Nanowires. *Nano Lett.* **2011**, *11*, 2424−2429.

(13) Cirlin, G. E.; Dubrovskii, V. G.; Samsonenko, Y. B.; Bouravleuv, A. D.; Durose, K.; Proskuryakov, Y. Y.; Mendes, B.; Bowen, L.; Kaliteevski, M. A.; Abram, R. A.; Zeze, D. Self-catalyzed, pure zincblende GaAs nanowires grown on Si(111) by molecular beam epitaxy. *Phys. Rev. B* **2010**, *82*, 035302−6.

(14) Glas, F.; Harmand, J. C.; Patriarche, G. Why does wurtzite form in nanowires of III-V zinc blende semiconductors? *Phys. Rev. Lett.* **2007**, *99*, 146101.

(15) Caroff, P.; Dick, K. A.; Johansson, J.; Messing, M. E.; Deppert, K.; Samuelson, L. Controlled polytypic and twin-plane superlattices in III-V nanowires. *Nat. Nanotechnol.* **2009**, *4*, 50−55.

(16) Johansson, J.; Dick, K. A.; Caroff, P.; Messing, M. E.; Bolinsson, J.; Deppert, K.; Samuelson, L. Diameter Dependence of the Wurtzite−Zinc Blende Transition in InAs Nanowires. *J. Phys. Chem. C* **2010**, *114*, 3837−3842.

(17) Joyce, H. J.; Wong-Leung, J.; Gao, Q.; Tan, H. H.; Jagadish, C. Phase Perfection in Zinc Blende and Wurtzite III-V Nanowires Using Basic Growth Parameters. *Nano Lett.* **2010**, *10*, 908−915.

(18) Paiman, S.; Gao, Q.; Joyce, H. J.; Kim, Y.; Tan, H. H.; Jagadish, C.; Zhang, X.; Guo, Y.; Zou, J. Growth temperature and V/III ratio effects on the morphology and crystal structure of InP nanowires. *J. Phys. D: Appl. Phys.* **2010**, *43*, 445402.

(19) Johansson, J.; Karlsson, L. S.; Dick, K. A.; Bolinsson, J.; Wacaser, B. A.; Deppert, K.; Samuelson, L. Effects of Supersaturation on the Crystal Structure of Gold Seeded III-V Nanowires. *Cryst. Growth Design* **2009**, *9*, 766−773.

(20) Thelander, C.; Dick, K. A.; Borgstrom, M. T.; Froberg, L. E.; Caroff, P.; Nilsson, H. A.; Samuelson, L. The electrical and structural properties of n-type InAs nanowires grown from metal-organic precursors. *Nanotechnology* **2010**, *21*, 205703.

(21) Algra, R. E.; Verheijen, M. A.; Borgstrom, M. T.; Feiner, L. F.; Immink, G.; van Enckevort, W. J. P.; Vlieg, E.; Bakkers, E. Twinning superlattices in indium phosphide nanowires. *Nature* **2008**, *456*, 369−372.

(22) Wallentin, J.; Ek, M.; Wallenberg, L. R.; Samuelson, L.; Deppert, K.; Borgstrom, M. T. Changes in Contact Angle of Seed Particle Correlated with Increased Zincblende Formation in Doped InP Nanowires. *Nano Lett.* **2010**, *10*, 4807−4812.

(23) Caroff, P.; Wagner, J. B.; Dick, K. A.; Nilsson, H. A.; Jeppsson, M.; Deppert, K.; Samuelson, L.; Wallenberg, L. R.; Wernersson, L.-E. High-quality InAs/InSb nanowire heterostructures grown by metal−organic vapor-phase epitaxy. *Small* **2008**, *4*, 878−882.

(24) Xu, T.; Dick, K. A.; Plissard, S.; Nguyen, T. H.; Makoudi, Y.; Berthe, M.; Nys, J. P.; Wallart, X.; Grandidier, B.; Caroff, P. Faceting, composition and crystal phase evolution in III- V antimonide nanowire heterostructures revealed by combining microscopy techniques. *Nanotechnology* **2012**, *23*, 095702.

(25) Plissard, S.; Dick, K. A.; Wallart, X.; Caroff, P. Gold-free GaAs/GaAsSb heterostructure nanowires grown on silicon. *Appl. Phys. Lett.* **2010**, *96*, 121901−3.

(26) Dheeraj, D. L.; Patriarche, G.; Zhou, H. L.; Hoang, T. B.; Moses, A. F.; Gronsberg, S.; van Helvoort, A. T. J.; Fimland, B. O.; Weman, H. Growth and Characterization of Wurtzite GaAs Nanowires with Defect-Free Zinc Blende GaAsSb Inserts. *Nano Lett.* **2008**, *8*, 4459−4463.

(27) Fang, H.; Chuang, S.; Takei, K.; Kim, H. S.; Plis, E.; Liu, C. H.; Krishna, S.; Chueh, Y. L.; Javey, A. Ultrathin-body high-mobility InAsSb-on-insulator field-effect transistors. *IEEE Electron Device Lett.* **2012**, *33*, 504−506.

DOI: 10.1021/nl5040946
Nano Lett. 2015, 15, 1109−1116

(28) Sourribes, M. J. L.; Isakov, I.; Panfilova, M.; Liu, H.; Warburton, P. A. Mobility Enhancement by Sb-Mediated Minimization of Stacking Fault Density in InAs Nanowires Grown on Silicon. *Nano Lett.* **2014**, *14*, 1643−1650.
(29) Anyebe, E. A.; Zhuang, Q. Self-catalysed InAs1-xSbx nanowires grown directly on bare Si substrates. *Mater. Res. Bull.* **2014**, *60*, 572−575.
(30) Anyebe, E. A.; Rajpalke, M. K.; Veal, T. D.; Jin, C. J.; Wang, Z. M.; Zhuang, Q. D. Surfactant effect of antimony addition to the morphology of self-catalysed $InAs_{1-x}Sb_x$ nanowires. *Nano Res.* **2015**.
(31) Dimakis, E.; Lähnemann, J.; Jahn, U.; Breuer, S.; Hilse, M.; Geelhaar, L.; Riechert, H. Self-Asssisted Nucleation and Vapor−Solid Growth of InAs Nanowires on Bare Si(111). *Crys. Growth Designs* **2011**, *11*, 4001−4008.
(32) Wei, W.; Bao, X.-Y.; Soci, C.; Ding, Y.; Wang, Z.-L.; Wang, D. Direct Heteroepitaxy of Vertical InAs Nanowires on Si Substrates for Broad Band Photovoltaics and Photodetection. *Nano Lett.* **2009**, *9*, 2926−2934.
(33) Jing, Y.; Bao, X.; Wei, W.; Li, C.; Sun, K.; Aplin, D. P. R.; Ding, Y.; Wang, Z.-L.; Bando, Y.; Wang, D. Catalyst-Free Heteroepitaxial MOCVD Growth of InAs Nanowires on Si Substrates. *J. Phys. Chem. C* **2013**, *118*, 1696−1705.
(34) Akiyama, T.; Sano, K.; Nakamura, K.; Ito, T. An empirical potential approach to wurtzite-zinc-blende polytypism in group III-V semiconductor nanowires. *Jpn. J. Appl. Phys., Part 2* **2006**, *45*, L275−L278.
(35) Dubrovskii, V. G.; Sibirev, N. V. Growth thermodynamics of nanowires and its application to polytypism of zinc blende III- V nanowires. *Phys. Rev. B* **2008**, *77*, 035414−8.
(36) Du, W.-N.; Yang, X.-G.; Wang, X.-Y.; Pan, H.-Y.; Ji, H.-M.; Luo, S.; Yang, T.; Wang, Z.-G. The self-seeded growth of InAsSb nanowires on silicon by metal-organic vapor phase epitaxy. *J. Cryst. Growth* **2014**, *396*, 33−37.
(37) Borg, B. M.; Kimberly, A. D.; Joël, E.; Lars-Erik, W. Enhanced Sb incorporation in InAsSb nanowires grown by metalorganic vapor phase epitaxy. *Appl. Phys. Lett.* **2011**, *98*, 113104−3.
(38) Ercolani, D.; Gemmi, M.; Nasi, L.; Rossi, F.; Pea, M.; Li, A.; Salviati, G.; Beltram, F.; Sorba, L. Growth of InAs/ InAsSb heterostructured nanowires. *Nanotechnology.* **2012**, *23*, 115606−9.
(39) Pea, M.; Ercolani, D.; Li, A.; Gemmi, M.; Rossi, F.; Beltram, F.; Sorba, L. Suppression of lateral growth in InAs/ InAsSb heterostructured nanowires. *J. Cryst. Growth* **2013**, *366*, 8−14.
(40) Mandl, B.; Dick, K. A.; Kriegner, D.; Keplinger, M.; Bauer, G.; Stangl, J.; Deppert, K. Crystal structure control in Au-free self-seeded InSb wire growth. *Nanotechnology* **2011**, *22*, 145603.
(41) Krogstrup, P.; Popovitz-Biro, R.; Johnson, E.; Madsen, M. H.; Nygard, J.; Shtrikman, H. Structural phase control in self-catalyzed growth of GaAs nanowires on silicon (111). *Nano Lett.* **2010**, *10*, 4475−4482.
(42) Spirkoska, D.; Arbiol, J.; Gustafsson, A.; Conesa-Boj, S.; Glas, F.; Zardo, I.; Heigoldt, M.; Gass, M. H.; Bleloch, A. L.; Estrade, S.; Kaniber, M.; Rossler, J.; Peiro, F.; Morante, J. R.; Abstreiter, G.; Samuelson, L.; Morral, A. F. I., Structural and optical properties of high quality zinc-blende/wurtzite GaAs nanowire heterostructures. *Phys. Rev. B* **2009**, *80*.
(43) Plissard, S.; Dick, K. A.; Larrieu, G.; Godey, S.; Addad, A.; Wallart, X.; Caroff, P. Gold-free growth of GaAs nanowires on silicon: arrays and polytypism. *Nanotechnology* **2010**, *21*, 385602.
(44) Krogstrup, P.; Curiotto, S.; Johnson, E.; Aagesen, M.; Nygard, J.; Chatain, D. Impact of the liquid phase shape on the structure of III-V nanowires. *Phys. Rev. Lett.* **2011**, *106*, 125505−4.
(45) Leitsmann, R.; Bechstedt, F. Surface influence on stability and structure of hexagon-shaped III-V semiconductor nanorods. *J. Appl. Phys.* **2007**, *102*, 063528−8.
(46) Anyebe, E. A.; Zhuang, Q.; Sanchez, A.; Lawson, S.; Robson, A. J.; Ponomarenko, L.; Zhukov, A.; Kolosov, O. Self-catalysed growth of InAs nanowires on bare Si substrates by droplet epitaxy. *Rapid Res. Lett.* **2014**, *8*, 658−662.
(47) Dubrovskii, V. G.; Sibirev, N. V. Growth rate of a crystal facet of arbitrary size and growth kinetics of vertical nanowires. *Phys. Rev. E* **2004**, *70*, 031604−7.
(48) Borg, B. M.; Wernersson, L.-E. Synthesis and properties of antimonide nanowires. *Nanotechnology* **2013**, *24*, 202001.
(49) Algra, R. E.; Verheijen, M. A.; Feiner, L. F.; Immink, G. G. W.; van Enckevort, W. J. P.; Vlieg, E.; Bakkers, E. The Role of Surface Energies and Chemical Potential during Nanowire Growth. *Nano Lett.* **2011**, *11*, 1259−1264.
(50) Lehmann, S.; Wallentin, J.; Jacobsson, D.; Deppert, K.; Dick, K. A. A General Approach for Sharp Crystal Phase Switching in InAs, GaAs, InP, and GaP Nanowires Using Only Group V Flow. *Nano Lett.* **2013**, *13*, 4099−4105.
(51) Dubrovskii, V. G.; Sibirev, N. V.; Harmand, J. C.; Glas, F. Growth kinetics and crystal structure of semiconductor nanowires. *Phys. Rev. B* **2008**, *78*, 235301−10.
(52) Wallentin, J.; Mergenthaler, K.; Ek, M.; Wallenberg, L. R.; Samuelson, L.; Deppert, K.; Pistol, M.-E.; Borgstrom, M. T. Probing the Wurtzite Conduction Band Structure Using State Filling in Highly Doped InP Nanowires. *Nano Lett.* **2011**, *11*, 2286−2290.
(53) Kawaguchi, K.; Ekawa, M.; Akiyama, T.; Kuwatsuka, H.; Sugawara, M. Surfactant-Related Growth of $InAs_{1-x}Sb_x$ Quantum Structures on InP(001) by Metalorganic Vapor-Phase Epitaxy. *J. Cryst. Growth.* **2006**, *29*, 154−159.
(54) Sun, M. H.; Leong, E. S. P.; Chin, A. H.; Ning, C. Z.; Cirlin, G. E.; Samsonenko, Y. B.; Dubrovskii, V. G.; Chuang, L.; Chang-Hasnain, C. Photoluminescence properties of InAs nanowires grown on GaAs and Si substrates. *Nanotechnology* **2010**, *21*, 335705.
(55) Gladkov, P.; Nohavica, D.; Sourek, Z.; Litvinchuk, A. P.; Iliev, M. N. Growth and characterization of InAs layers obtained by liquid phase epitaxy from Bi solvents. *Semicond. Sci. Technol.* **2006**, *21*, 544−549.
(56) Koblmuller, G.; Vizbaras, K.; Hertenberger, S.; Bolte, S.; Rudolph, D.; Becker, J.; Doblinger, M.; Amann, M. C.; Finley, J. J.; Abstreiter, G. Diameter dependent optical emission properties of In As nanowires grown on Si. *Appl. Phys. Lett.* **2012**, *101*, 053103−5.
(57) Grober, R. D.; Drew, H. D.; Chyi, J. I.; Kalem, S.; Morkoc, H. Infrared photoluminescence of InAs epilayers grown on GaAs and Si substrates. *J. Appl. Phys.* **1989**, *65*, 4079−4081.
(58) Zhang, L. J.; Luo, J. W.; Zunger, A.; Akopian, N.; Zwiller, V.; Harmand, J. C. Wide InP nanowires with Wurtzite/Zincblende superlattice segments are type-II whereas narrower nanowires become type-I: an atomistic pseudopotential calculation. *Nano Lett.* **2010**, *10*, 4055−4060.
(59) Murayama, M.; Nakayama, T. Chemical trend of band offsets at wurtzite/ zinc- blende heterocrystalline semiconductor interfaces. *Phys. Rev. B* **1994**, *49*, 4710−4724.
(60) Fang, Z. M.; Ma, K. Y.; Jaw, D. H.; Cohen, R. M.; Stringfellow, G. B. Photoluminescence of InSb, InAs, and InAsSb grown by organometallic vapor phase epitaxy. *J. Appl. Phys.* **1990**, *67*, 7034−7039.
(61) Zanolli, Z.; Fuchs, F.; Furthmueller, J.; von Barth, U.; Bechstedt, F. Model GW band structure of InAs and GaAs in the wurtzite phase. *Phys. Rev. B* **2007**, *75*, 245121−8.
(62) Bao, J.; Bell, D. C.; Capasso, F.; Erdman, N.; Wei, D.; Froberg, L.; Martensson, T.; Samuelson, L. Nanowire-induced Wurtzite InAs thin film on Zinc-Blende InAs substrate. *Adv. Mater.* **2009**, *21*, 3654−3658.
(63) De, A.; Pryor, C. E. Predicted band structures of III-V semiconductors in the wurtzite phase. *Phys. Rev. B* **2011**, *84*, 155210−13.
(64) Vurgaftman, I.; Meyer, J. R.; Ram-Mohan, L. R. Band parameters for III-V compound semiconductors and their alloys. *J. Appl. Phys.* **2001**, *89*, 5815.

DOI: 10.1021/nl5040946
Nano Lett. 2015, 15, 1109−1116